

KIC 2856960: the impossible triple star

T. R. Marsh¹, D. J. Armstrong¹, P.J. Carter^{2,1}

¹*Department of Physics, University of Warwick, Gibbet Hill Road, Coventry, CV4 7AL, UK*

²*School of Physics, H.H. Wills Physics Laboratory, University of Bristol, Tyndall Avenue, Bristol BS8 1TL*

Accepted —. Received —; in original form —

ABSTRACT

KIC 2856960 is a star in the *Kepler* field which was observed by *Kepler* for 4 years. It shows the primary and secondary eclipses of a close binary of period 0.258 d as well as complex dipping events that last for about 1.5 d at a time and recur on a 204 d period. The dips are thought to result when the close binary passes across the face of a third star. In this paper we present an attempt to model the dips. Despite the apparent simplicity of the system and strenuous efforts to find a solution, we find that we cannot match the dips with a triple star while satisfying Kepler’s laws. The problem is that to match the dips the separation of the close binary has to be larger than possible relative to the outer orbit given the orbital periods. Quadruple star models can get round this problem but require the addition of a so-far undetected intermediate period of order 5 – 20 d that has to be a near-perfect integer divisor of the outer 204 d period. Although we have no good explanation for KIC 2856960, using the full set of *Kepler* data we are able to update several of its parameters. We also present a spectrum showing that KIC 2856960 is dominated by light from a K3- or K4-type star.

Key words: (stars:) binaries (including multiple:) close – (stars:) binaries: eclipsing

1 INTRODUCTION

A large fraction of stars are found in binary systems, and a significant number of binary stars reside in triple systems. Triple stars add complexity to the dynamics and evolution of stars (Naoz et al. 2013; Eggleton & Kiseleva-Eggleton 2001). Even though binary stars offer many outcomes closed to single star evolution, there are systems where evolution within a triple is the simplest explanation for otherwise puzzling data (O’Brien et al. 2001), and location within triple systems has been suggested as a way to speed the merger of compact objects, which might help drive Type Ia supernovae and other exotic transients (Thompson 2011). Triple stars are mini-clusters, with three co-eval stars in orbits which, in favourable circumstances, may allow us to determine precision fundamental parameters for all three objects.

Eclipsing systems are a well-travelled route to precision stellar parameters. In the case of triple systems there are three different pairs of stars that can eclipse, but the chances of suitably aligned systems are low, given the hierarchical structure of triples which contain binary stars in much longer period and therefore wider orbits with third stars. Fortunately, the nearly uninterrupted coverage provided by the *Kepler* satellite has uncovered a significant number of triples (Gies et al. 2012; Rappaport et al. 2013; Conroy et al. 2014), and a number of these are multiply eclipsing. Examples are KOI-126, which has a 1.77 d close binary in a 33.9 d orbit with a third star (Carter et al. 2011), and HD 181068, which contains a 0.90 d binary in a 45 d orbit with a red giant (Derekas et al. 2011). KOI-126 in particular led to precise masses and radii of all three component stars.

KIC 2856960 is another eclipsing triple star observed by *Kepler*. Listed as an eclipsing binary by Prša et al. (2011), KIC 2856960 was subsequently found to be a triple system after the discovery of a second set of eclipses in addition to those of the binary (Armstrong et al. 2012). The binary in KIC 2856960 reveals itself through $\sim 1\%$ -deep eclipses (primary and secondary) on a period of 0.258 d. Its triple nature is apparent from complex clusters of dips in flux up to 8% deep, which last for a little over one day at each appearance, and recur on a period of ~ 204 d (Armstrong et al. 2012; Lee et al. 2013). Armstrong et al. (2012) suggested two very different models for the system. In the first, the dip clusters are produced when a dim circumbinary object, possibly a planet, passes in front of the close binary, with multiple eclipses taking place as the binary completes its orbits. In the second, it is the close binary passing across the face of a third star that produces the dips. The second model was proven correct by Lee et al. (2013) who found variations in the times of the eclipses of the close binary consistent with light travel time variations as it orbited a third star. Thus KIC 2856960 has all the characteristics of a hierarchical triple, with a close binary of a period ~ 0.258 d in a 204 d period orbit with a third star.

There has been no analysis of KIC 2856960 to see if, like KOI-126, it can yield precision parameters of its component stars. Here we document our efforts to do this, efforts which ended in failure. Not only do we not find a precision set of masses and radii for the component stars, we do not find *any* physically-consistent set of masses and radii that comes close to explaining KIC 2856960’s light curve. The nature of the disagreement leads us to conclude that, despite appearances, KIC 2856960 cannot be modelled as a

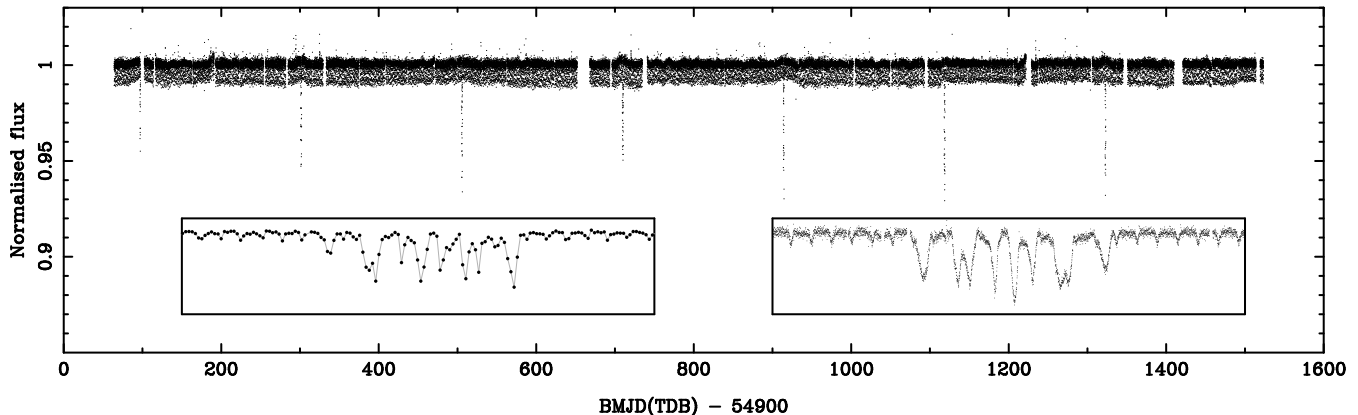


Figure 1. The light-curve of KIC 2856960 observed by *Kepler*. This spans 4 years and was mostly taken in long cadence (30 min sampling) mode. The main section of short cadence (1 min) data runs from 1100 to 1300 d on the plot, with an additional short section at the end. For clarity, the data were binned in a way which does not affect the long cadence data, but placed the short cadence data onto a similar sampling (50 points per day). The seven narrow dropouts are the “dips”. The insets show 3 day-long zoomed plots around the third set of dips centred at 505 d (left) and the sixth set of dips at 1119 d (right), the only one observed in short cadence. The latter zoomed section is displayed at the full short-cadence resolution. Each zoom runs vertically from 0.90 to 1.02. In the left-hand zoom, we join the dots to make the dips clearer. Data away from the dips has a bi-modal appearance caused by the binary eclipses which can also be seen in the insets.

triple star. Here we describe why we are led to this conclusion, and tentatively propose quadrupole star models as a possible escape route.

2 OBSERVATIONS

The NASA *Kepler* satellite is a mission producing extremely high precision, near continuous light curves of $\sim 155,000$ stars on the level of 20 ppm Koch et al. (2010); Batalha et al. (2010); Koch et al. (2010). The mission began science operations on 13 May 2009.

Kepler added significant new data on KIC 2856960 to those published by Armstrong et al. (2012); Lee et al. (2013). Particularly significant are somewhat more than two quarters of short cadence (1 minute) data which fully resolve both the binary eclipses and one set of dips, compared to the majority of the data which were taken in long cadence mode (30 minutes). Sadly, *Kepler* suffered a failure of one its reaction wheels shortly before a second set of dips were to be observed in short cadence, terminating its coverage of KIC 2856960. This left 1500 d of data publicly available on the NASA Data Archive¹, from which we sourced the light curve of KIC 2856960. Detrending of the data was performed by the *Kepler* science team using the Pre-search Data Conditioning pipeline (PDC-MAP, see Stumpe et al. (2012) for an overview and examples, and Smith et al. (2012) for a full description of the detrending process).

We obtained spectra of KIC 2856960 in service mode on the night of May 21, 2012. The spectra were acquired with the ISIS spectrograph on the 4.2m William Herschel Telescope at the Roque de Los Muchachos on the island of La Palma in the Canary Islands. ISIS uses a dichroic and two separate arms to cover blue and red wavelengths simultaneously. We used the 600 lines/mm gratings to cover the wavelength ranges 370 to 530 nm and 565 to 735 nm at resolutions of 0.20 and 0.18 nm respectively, with around 4 pixels per resolution element. We took two spectra in each arm with

1200 s exposures, separated by 3 hours in time. There was no difference or radial velocity shift between the spectra so we combined them into one with 2400 s total exposure in each arm.

3 ANALYSIS

3.1 An overview of the light-curve of KIC 2856960

Fig. 1 displays an overview of the *Kepler* light-curve of KIC 2856960. For most of the time, the light-curve displays $\sim 1\%$ deep eclipses which repeat every 0.129 d which are the primary and secondary eclipses of a $P = 0.258$ d binary star. KIC 2856960 would be unremarkable were it not for seven brief intervals during which the flux dips up to 8% below its normal level. These are the “dips”, previously referred to, which recur every 204 d. As the insets of two of these dips show, they have a complex structure in which the flux sometimes returns to its normal level between dips and each cluster contains up to 9 minima. Our aim is to try to elucidate how these structures come about.

3.2 The close binary and its orbit within the triple

We begin our analysis by looking at the close binary light curve and the light travel time variations. These are the most secure aspect of the system, and given the difficulties we encounter understanding the dips, it is desirable in the first instance to understand as much a possible about the light-curve away from the dips. This is a repeat of the work of Lee et al. (2013) but with the considerable advantage of the short cadence data which allows us to resolve the binary eclipses. Before starting, we first define all the parameters that define the triple star model (Table 1). We adopt the convention that the $P = 0.258$ d close binary and its orbit will be referred to as “the binary”, while the $P = 204$ d long period outer orbit will be called “the triple”. We will exclusively use the symbols defined in Table 1. These differ in some respects from those defined by Lee et al. (2013) and care should be taken when comparing our values to theirs. When we quote their values, we have translated the symbols they used into our convention. We define the “ascending node”

¹ <http://archive.stsci.edu/kepler/>

Name	Unit	Description	Comment
R_1	R_\odot	Radius of star 1 of the binary	
R_2	R_\odot	Radius of star 2 of the binary	
R_3	R_\odot	Radius of star 3, the tertiary component of the system	
a_1	R_\odot	Semi-major axis of star 1 within the binary	
a_2	R_\odot	Semi-major axis of star 2 within the binary	
a_3	R_\odot	Semi-major axis of star 3 within the triple	
a_b	R_\odot	Semi-major axis of binary within the triple	
i_b	degrees	Orbital inclination of the binary	
i_t	degrees	Orbital inclination of the triple	
T_b	days	Epoch of primary eclipse of close binary, star 1 transiting star 2, MJD(BTDB)	
T_t	days	Epoch of the dips, close binary transiting star 3, MJD(BTDB)	
P_b	days	Orbital period of the binary	
P_t	days	Orbital period of the triple	
Ω_b	degrees	Longitude of ascending node of the binary	
Ω_t	degrees	Longitude of ascending node of the triple	Fixed to 270°
e_b	—	eccentricity of the binary	Fixed to 0
e_t	—	eccentricity of the triple	
ω_b	degrees	Longitude of periastron of the binary	Fixed to 0°
ω_t	degrees	Longitude of periastron of the triple	
S_1	R_\odot^{-2}	Central surface brightness, star 1	
S_2	R_\odot^{-2}	Central surface brightness, star 2	
S_3	R_\odot^{-2}	Central surface brightness, star 3	
u_1	—	Linear limb darkening coefficient, star 1	Fixed to 0.5
u_2	—	Linear limb darkening coefficient, star 2	Fixed to 0.5
u_3	—	Linear limb darkening coefficient, star 3	Fixed to 0.5
l_3	—	“Third light” as a fraction of total flux	

Table 1. Physical parameters defining the triple star model.

to be the point in an orbit when a star lies in the plane of the sky that contains the focus of its orbit and is travelling away from the observer.

Lee et al. (2013) used the first 6 quarters of *Kepler* data on KIC 2856960, all taken in long cadence. They modelled the binary light curve with two tidally-distorted stars in Roche geometry, finding that it matches a pair of low-mass M dwarfs, but with a 97% “third light” contribution, which they ascribed to the third star. Importantly, they found that the eclipse times of the binary exhibited a large periodic variation, on the same period (204 d) as the dips. This variation can only be explained through light travel time variations. The orbit defined by the light travel time variations was one of high eccentricity with $e_t = 0.612 \pm 0.082$, and a periastron angle indicating that the major-axis of the ellipse lies close to the plane of the sky. Fig. 2 shows the phase-folded light curve of the short cadence data taken towards the end of *Kepler*’s coverage of KIC 2856960. The variations outside eclipse are suggestive of star spots. Fig. 3 shows phase-folded light curves from data in 20 time intervals from the start to the end of the 4 years of *Kepler* data. The sharper short-cadence dominated curves are visible towards the top of the plot. There is significant variability between the light curves which is presumably the result of changes in spot coverage and location. The overall impression from Figs 2 and 3 is of a fairly typical, late-type, main-sequence eclipsing binary.

Our main interest in analysing the binary on its own is to establish as many parameters as possible that can be held fixed in subsequent fits to the dips. While a simultaneous fit of all parameters would be preferable, it turns out that even for our best models the dips and the binary eclipses each point towards very different values of some parameters. Examples are the ratio of radii of the two stars of the close binary and its epoch of zero phase. These are a few of several indications that our model of the dips must be wrong. Therefore, starting from the premise that we understand the

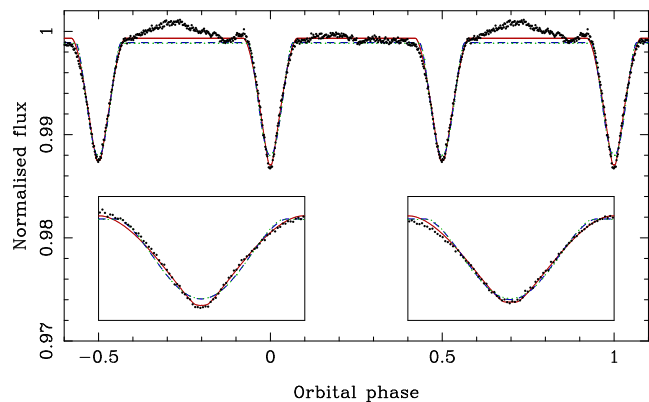


Figure 2. The short cadence data of KIC 2856960 (291505 points) folded on the 0.258 d period of the close binary, excluding data affected by the dips, and corrected for light-travel time variations induced by its orbit within the triple system. The data have been averaged into 500 bins per orbit. Phase 0 is defined by the slightly deeper primary eclipse. While there are some signs of tidally-induced ellipsoidal modulations outside the eclipses, these are largely masked by what are probably starspot-induced variations. Insets show horizontally-expanded views of the primary (left) and secondary (right) eclipses. The solid line shows a best-fitting model based upon two limb-darkened spheres. This has a radius ratio $R_1/R_2 = 0.88$. The dashed and dotted lines show models of the same total eclipse width but with the radius ratio held fixed at $R_1/R_2 = 2$ and $R_1/R_2 = 4$ respectively.

binary better than the dips, we adopt the approach of letting the binary data fix as many parameters as possible, before attempting to model the dips. We used the same code as we later use in fitting the dips and will defer a description of the methods until then.

As part of fitting the binary’s light curve, we had to allow for

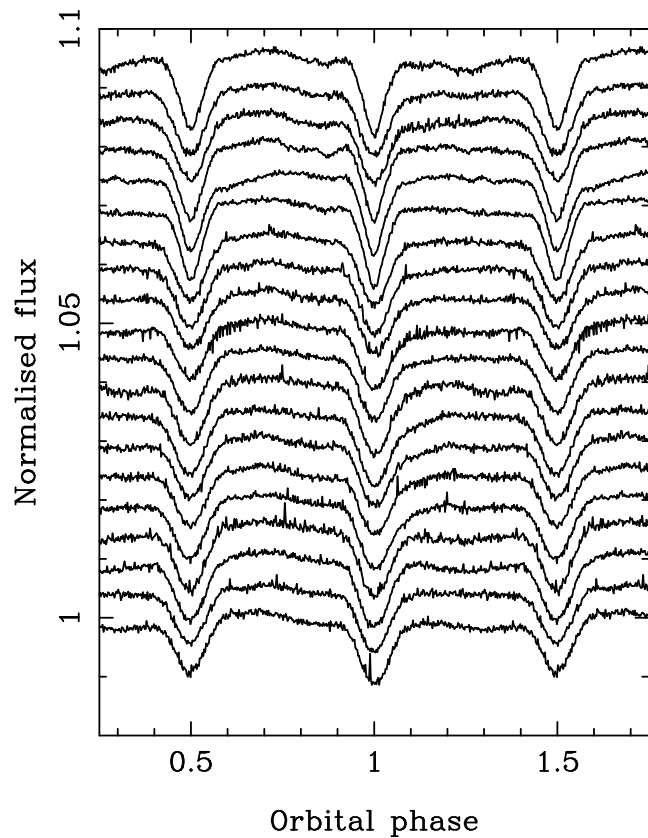


Figure 3. The close binary light curve folded in 20 time intervals spread equally from start to end of the *Kepler* observations of KIC 2856960. Time increases upwards. The topmost light curve and those 3 to 5 places down from it are derived from short-cadence data. There are obvious variations of shape outside the eclipse, e.g. the light curve fifth from the top. The light curves are offset vertically by 0.005.

the timing variations caused by its orbit within the triple, therefore the parameters associated with the triple orbit are a natural by-product of the light curve modelling. In order to show the effect of the triple star’s orbit, we measured the epoch of the binary over small intervals (roughly five days) of time throughout the *Kepler* observations. The results, along with the fit derived from the binary light curve analysis are shown in Fig. 4. The variations seen are highly significant. The dips occur close to the time when the binary is closest to us, so that we see its eclipses arrive early. There can be no doubt over Lee et al. (2013)’s conclusions that the binary is in an eccentric orbit with another object and that the dips occur when it passes in front of that object.

The parameters derived from the fits to the binary and its orbit within the triple are listed in Table 2. We did not determine the triple ephemeris from the binary data as it is more precisely pinned down by the dips (see section 3.6). Where possible we list the equivalent values from Lee et al. (2013), although our two models are not precisely the same since they used a more sophisticated model accounting for tidal deformation, gravity darkening and star spots, which, for reasons of compatibility with the triple star models to be described later, we do not apply. We believe that in any case the degeneracy associated with the spots limits the accuracy with which some parameters can be determined, as we will detail shortly. It should be noted that we truncated the distribution of i_b at 90° where it peaks. We distinguish between those pa-

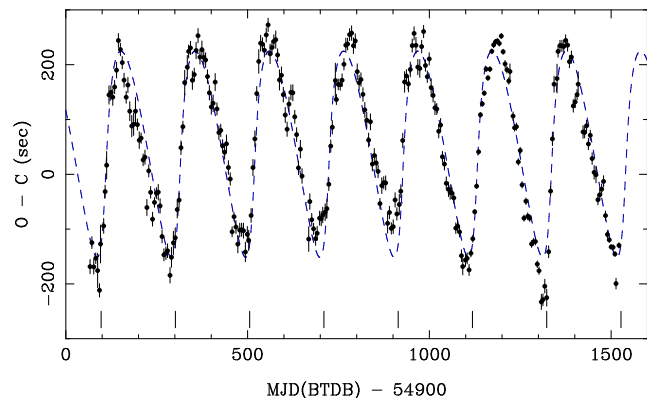


Figure 4. The observed times of the binary eclipses minus those calculated assuming a constant period show a large modulation due to the binary’s orbit with a third object. The dashed line shows an eccentric orbit fit which was established from a light-curve to all the data excluding those affected by dips. The times plotted were calculated by holding all parameters fixed apart from the binary’s zeropoint and fitting to 280 sub-sections of data, equally spaced from start to finish. The vertical lines at the bottom mark the mid-times of the dips (*Kepler* stopped observing KIC 2856960 just before the last one indicated). For reference, light takes 499 s to travel 1 AU.

Name	Value	Lee et al
T_b	55632.530537(34)	55632.53016(14)
P_b [d]	0.2585073013(50)	0.25850790(12)
$a_b \sin i_t$ [R_\odot]	99.38(70)	97(9)
e_t	0.6011(57)	0.612(82)
ω_t [$^\circ$]	344.64(64)	353(4)
$R_1/(a_1 + a_2)$	0.2485(6)	0.2041(45)
$R_2/(a_1 + a_2)$	0.2268(8)	0.3115(30)
i_b	$89.66(24)^\circ$	$85.32(66)^\circ$
S_2/S_1	1.155(2)	—
l_3	0.97235(6)	0.972(1)

Table 2. Parameters describing the inner binary and its orbit within the triple derived from a fit to all the data excluding the triple star dips.

rameters which describe the binary’s ephemeris and the orbit of its centre of mass within the triple (T_b , P_b , a_b , e_t and ω_t) and those which control the shape of the light curve, (the scaled radii $r_1 = R_1/(a_1 + a_2)$ and $r_2 = R_2/(a_1 + a_2)$, i_b , S_2/S_1 and l_3). The first set depend upon timing information, and can only be fixed by a fit to the whole light curve. When we come later to fit the dips, we will hold these fixed since any individual set of dips contains little information to constrain them (with the possible exception of T_b and P_b – see section 3.6). In contrast the dips are highly sensitive to r_1 , r_2 , etc, which we will call the shape parameters.

The shape parameters are not nearly as well constrained as the purely statistical uncertainties listed in Table 2 suggest because of distortion of the light curve, which like Lee et al. (2013), we put down to star spots. The effect of these is obvious outside eclipse in Figs 2 and 3. It can be seen quantitatively in the poor agreement between our radius values and those of Lee et al. (2013), and even amongst different fits of our model. For instance, we obtain an overall radius ratio (Table 2) of $R_1/R_2 = 1.10$, but when fitting to the short-cadence data alone we find $R_1/R_2 = 0.88$ (Fig. 2).

We focus on the radius ratio in particular because it turns out that to fit the dips we need much more extreme radius ratios than the values listed in Table 2 suggest. In Fig. 2 we show three model light

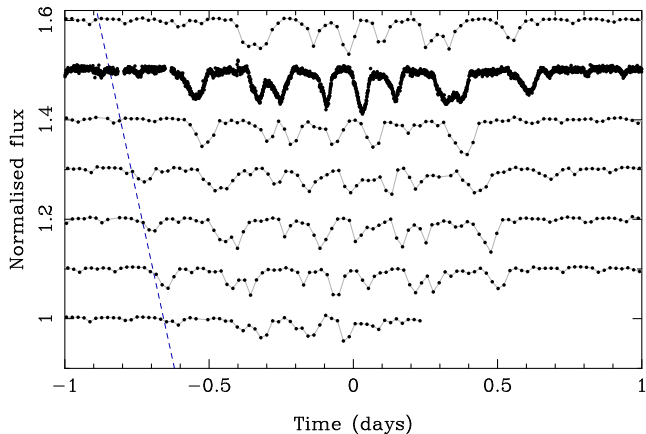


Figure 5. The seven consecutive dips in KIC 2856960 observed by *Kepler*, with time running upwards. Each has been aligned on the triple star ephemeris. From one set of dips to the next, the same dips are seen to recur, but to arrive earlier relative to the triple star ephemeris, as indicated by the dashed line which runs along the left-edge of the earliest dips seen in the second, third, fourth, and possibly also the first, set of dips.

curves. The solid line model shows a best fit with all the shape parameters allowed to vary. This led to $R_1/R_2 = 0.88$ and an almost edge-on inclination. For the other two we force large radius ratios $R_1/R_2 = 2$ and $R_1/R_2 = 4$ (which also forced much lower inclinations of 74° and 54° respectively). Our object in plotting these is to show that even large changes in the shape parameters, which are well outside the statistical uncertainties of Table 2, lead to relatively small changes in the light curves which are comparable to the spot-induced variations. This reflects a well-known degeneracy for partially-eclipsing, or almost partially-eclipsing binaries. As a result when we fit the dips, we do not restrict the shape parameters to the values listed in Table 2 but merely apply the following constraint that ensures that eclipses of the correct total width, $\Delta\phi = 0.155$ occur:

$$(r_1 + r_2)^2 = \cos^2 i_b + \sin^2 i_b \sin^2(\pi\Delta\phi). \quad (1)$$

Systematics are also visible in the light travel times of Fig. 4. It again seems likely that these reflect the spot-induced variability evident in Fig. 3. Although we weighted our fits towards the eclipses (since in our model the region out-of-eclipse contains no useful information on the timing), we can still expect the eclipses themselves to be affected by star spots. Given that the orbital period is 22300 s, and the level of variability in the light curves, the 20 – 50 s systematic deviations seen in Fig. 4 are understandable. Having established the triple’s orbit and the nature of the close binary star’s light curve, we now begin our analysis of the dips.

3.3 The Dips

3.3.1 Overview of the Dip light curves

We start with a qualitative, model-independent assessment of the light curves during the appearance of the dips. Fig. 5 shows all seven of the occurrences of the dips observed by *Kepler*. No two sets of dips are identical, but many bear strong similarities to each other. For instance, counting from the bottom, the second, third and sixth sets are very similar to each other, with each showing first a single dip, followed by a closely-spaced double dip, then by three somewhat more widely spaced dips, then another double dip and then a final single dip. The pattern of dips of one set can be seen to

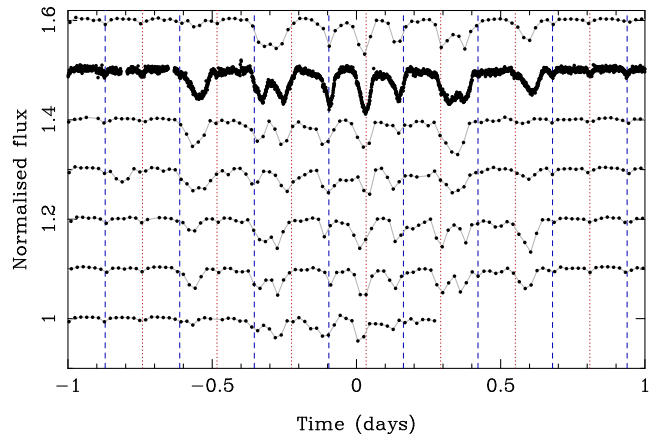


Figure 6. The same as Fig. 5, except now the times have been adjusted to the nearest binary cycle. Dashed lines mark binary phase 0; dotted lines mark binary phase 0.5.

arrive slightly earlier at the next set, as indicated by the dashed line in fig. 5. This can’t happen while maintaining a lock to the triple orbit without the dips evolving, and this can be seen as early arrivals fade away on the left-hand side of Fig. 5 just as new dips grow in strength on the right-hand side. (The situation is reminiscent of the behaviour of wave crests in groups of ripples on the surface of a pond.) The earliest any dip is seen is in the fourth event at around -0.72 d; the latest is also the fourth event at around $+0.72$ d, so the total duration of the dips exceeds 1.4 d.

In Fig. 6, we show the dips again but now with the times adjusted to the binary phase. This plot shows some very interesting features. First, the dips are stable relative to the binary phase. Second we see that the first dip in a given set always occurs during the binary phase interval 0.0 to 0.5, while the last always occurs in the interval 0.5 to 1.0. Moreover, no dip is seen in the half cycle following the first dip, or in the half cycle preceding the last dip. This is *extremely odd*. In the previous section, we showed that the two components of the binary have similar radii, so it should look very similar at any two phases 0.5 cycles apart. However it seems instead that in one configuration obscuration occurs while it does not in the other. It is as if only one of the two stars in the binary occults the third object.

In contrast to the half-cycle following the first dip in a set, which seems to be free of any obscuration, the half cycle following the double dip (covering around -0.22 to -0.1 dcd in Fig. 6) is usually not entirely clean, but shows some slight slopes. The half cycle preceding the final double dip behaves similarly. These are perhaps small signs of the presence of star 2, although the contrast between successive half cycles is still much stronger than the binary model would suggest.

3.3.2 Modelling the Dips

In order to model the dips, we developed a model of a triple star involving three limb-darkened spheres, in hierarchical Keplerian orbits, specified by the parameters listed in Table 1. Our concern here is to capture the main features of the data and we do not include effects of secondary importance (for KIC 2856960 at least) such as tidal distortion and gravity darkening. This considerably speeds the computations, which are a limiting factor in much of the modelling. We do not account for N -body corrections to the Keplerian orbits because we expect these to be small given the ~ 800 -fold ratio of

the outer and inner orbital periods. To compute the flux from each star, its circular projected face was split into a set of concentric annuli of constant radial increment but variable surface brightness because of limb darkening. The task then breaks down to working out how much of each annulus is visible given the locations and sizes of the other two stars. The number of annuli determines the extent of numerical noise. We used 80 for each star, verifying that the resultant numerical noise was less than the noise level in the data. The only notable feature of the parameters chosen is our choice of zeropoints, T_b and T_t , which mark central times of the binary star’s primary eclipses on the one hand and the “dips” on the other, as opposed to the more usual time of periastron passage. We made this choice because the eclipse and event times are more-or-less directly fixed by the data. This means that the resulting epochs are much less correlated with other parameters than they would have been had we used the periastron times instead. We tested the code by verifying that it correctly reproduced the light curve of the triple system KOI-126 at the epoch closest to the epoch of the orbital elements quoted by Carter et al. (2011).

Later on we will examine quadruple star models for KIC 2856960, making the geometry harder to visualise. Therefore in Fig. 7 we give schematic pictures of the three types of orbits that we will consider. The observer is assumed to be in the plane of the figure, looking from below, and the system is shown at the time of the dips.

We varied or fixed parameters according to whether the data significantly constrained them. For instance, we set $\Omega_t = 270^\circ$ (ascending node due West on the sky, in the usual direction of the x -axis) from the start since there is no information upon the absolute orientation of the system. On the other hand, the data strongly constrain the relative orientation the binary and triple, so Ω_b was allowed to vary. Similarly, the limb darkening coefficients were uniformly set equal to 0.5 since they have a relatively minor effect upon the light curves. In the case of the binary, the nature of its light curve and its short period very much suggest that it has a circular orbit, and so we fixed $e_b = 0$ and $\omega_b = 0$ for all models. Finally when fitting to data, we scaled the fluxes to minimise χ^2 as this is a fast operation. This meant that one of the surface brightness parameters could be fixed (since otherwise there would degeneracy between the surface brightnesses and the scaling factor), leaving us with a maximum of 18 parameters that could be varied.

As previously explained, owing to clear differences between the parameter space favoured by the binary light curve compared to the dips, we first fitted those parameters which could be determined from the binary alone. Thus we fixed T_b and P_b which define the binary’s ephemeris, and a_b , e_t and ω_t which define the triple orbit, to the values listed in the top section of Table 2. We will see later that all lengths in the system scale with the value of $a_b + a_3$, the semi-major axis of the triple, and masses therefore scale as $(a_b + a_3)^3$. While a_b is fixed by the light travel times (given that $\sin i_t = 1$ to a good approximation), we have no direct information upon a_3 , although it can be estimated by seeking a consistent set of masses and radii for the binary star, assuming it to be composed of a pair of M dwarfs. This is because the binary light curve fixes the radii scaled by the total separation, the masses scale as the total separation cubed, while the mass and radius of low mass stars are nearly linearly related (Torres 2013). Assuming a precise linear relation, $M/M_\odot = R/R_\odot$, and starting from the values listed in Table 2 leads to an estimate for $a_3 \approx 75 R_\odot$. We therefore adopt a round number of similar magnitude, and henceforth will assume that $a_3 = 100 R_\odot$. Where relevant later, we point out aspects that depend upon the particular value chosen for a_3 .

We carried out the fitting through a combination of standard minimisation methods (Nelder & Mead 1965; Powell 1964) and (mainly) Markov Chain Monte Carlo (MCMC) iteration. MCMC takes a Bayesian point of view whereby one constructs models that are distributed with the posterior probability distribution of the parameters, given the data. The posterior probability has prior probabilities representing one’s knowledge before any data are taken times the probability of the data given the model. The latter is encapsulated by χ^2 in our case since we assume independent gaussian uncertainties on the data. The prior provides a flexible way to impose physical constraints without requiring that they hold precisely at all times during minimisation. The most important such constraint comes from Kepler’s laws. We implemented our model with a combination of C and Python, and used the `emcee` package (Foreman-Mackey et al. 2013) to manage the MCMC computations.

Kepler’s third law applied to the triple orbit gives us the total system mass in terms of the controlling scale factor, $a_3 + a_b$:

$$G(m_1 + m_2 + m_3) = n_t^2 (a_3 + a_b)^3, \quad (2)$$

where $n_t = 2\pi/P_t$. The centre-of-mass condition

$$m_3 a_3 = (m_1 + m_2) a_b, \quad (3)$$

then allows us to deduce the mass of each component of the triple. A second application of Kepler’s third law then fixes the total separation of the binary

$$G(m_1 + m_2) = n_b^2 (a_1 + a_2)^3, \quad (4)$$

where $n_b = 2\pi/P_b$. Thus the value of $a_1 + a_2$ is fixed once $a_3 + a_b$ is fixed and cannot be allowed to vary independently of it. This we ensured through the prior probability by demanding near-equality between the value of $a_1 + a_2$ computed as above starting from $a_3 + a_b$ and the value derived from the models proposed during the MCMC process. Inequality was punished through low prior probability. This method allows great flexibility in terms of what is allowed to vary, whilst ensuring physical consistency. The degree of equality demanded, which has some impact upon the MCMC efficiency, could be tuned at will.

Fixing what parameters we could from the binary model, setting $a_3 = 100 R_\odot$, we went ahead and optimised the remaining 12 parameters which were the stellar radii R_1 , R_2 and R_3 , the binary semi-major axes a_1 and a_2 , the orbital inclinations i_b and i_t , the epoch of the triple T_t , the surface brightness parameters S_1 and S_2 along with the “third light” l_3 , and the orientation of the binary orbit, Ω_b . We applied Kepler’s laws via the prior as just outlined, and the constraint upon r_1 , r_2 and i_b to match the eclipse width that we described in section 3.2. The best fit to the short cadence dips resulting from this procedure is shown in the left-hand panel of Fig. 8. Clearly “best” is very much a relative term here as the fit is extremely poor with $\chi^2 \approx 60000$ for 4589 points. In particular the level of modulation in the central part of the dips is much weaker in the model than the data. This is because in the model $R_3 \approx 3.9 R_\odot$ is large compared to $R_1 = 1.29 R_\odot$ and $a_1 = 1.85 R_\odot$. Once the binary starts to cross star 3, one part of it is always in an occulting position. Besides providing a poor fit, the parameters that lead to the fit shown in Fig. 8 can be ruled out on astrophysical grounds. For instance star 1 ends up with almost zero mass ($10^{-5} M_\odot$) but a radius of $1.29 R_\odot$ (and thus overfills its Roche lobe).

Despite the poor fit, the model does show some similarities to the data indicating that it contains elements of truth. A much better although still imperfect fit ($\chi^2 = 13900$) is obtained if the Keplerian constraint is removed, as shown in the right-hand panel

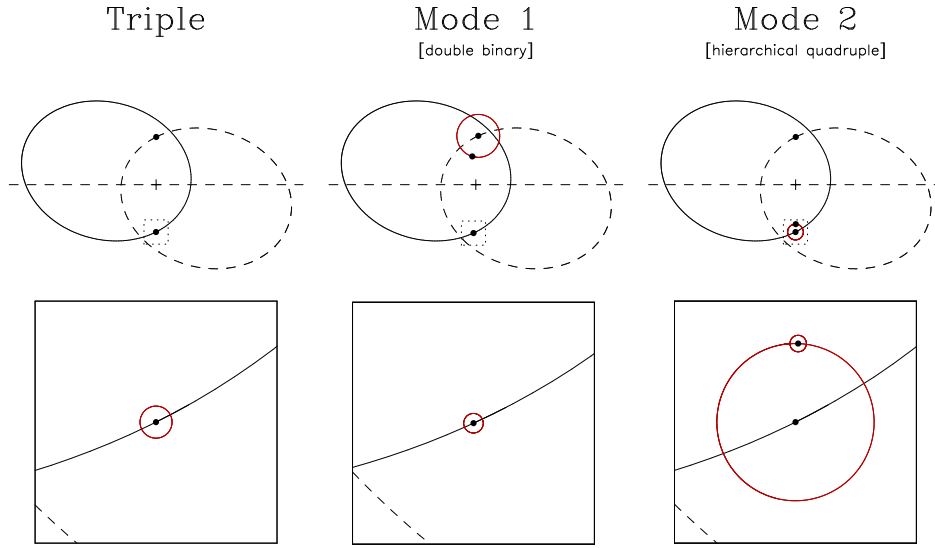


Figure 7. A face-on view of the three types of orbits (one triple, two quadruple) we consider for KIC 2856960, all drawn to scale with tilts removed so that there is no distortion by projection. The observer is assumed to lie in the plane of the figure and view the orbits edge-on from the bottom of the page. The horizontal dashed line represents the plane of the sky, with the '+' signs marking the system's centre of mass. The two ellipses show the centre of mass of the close binary in the left two panels (solid) and star 3 in the left- and right-hand panels (dashed). The lower panels show factor 10 magnified views of the regions delineated by small dotted squares centred near the close binary. In the central panel, the dashed ellipse shows the centre of mass of a second binary formed from star 3, the star that is eclipsed during the dips, and an extra star, "star 4", introduced in order to alter the dynamics for reasons explained in the text. The upper circle shows the orbit of star 3 around a fixed point on the dashed ellipse. All orbits are traversed counter-clockwise in this figure, so that in the configuration shown, which matches the time of the dips, the relative transverse speed between star 3 and the close binary is slowed by stars 3's motion within its binary with star 4. In the right-hand panel the solid-lined ellipse shows the track of the centre of mass of an inner triple made up of the close binary and "star 4", once more introduced to alter the dynamics of the system, but in a different configuration. The close binary thus moves on a circle around this guiding centre, as indicated by the large circle in the right-hand magnified view. The small circles, which can only be seen in the magnified views, represent the orbit of star 1 (again with its guiding centre held stationary at the time of the dips). Dots in each panel show the centre of mass of the close binary and star 3. Additionally, in the centre panel the dot on the dashed ellipse represents the centre of mass of the second binary, while in the right-hand panel the dot on the solid ellipse marks the centre of mass of the inner triple. The orbits of stars 2 and 4 are suppressed for clarity.

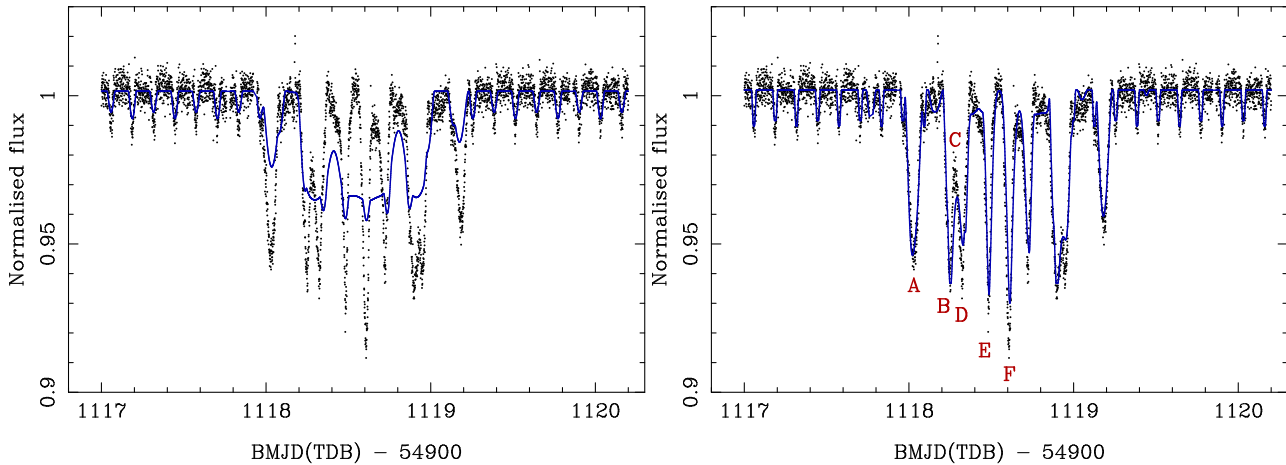


Figure 8. *Left-panel:* The set of dips observed in short cadence along with the best fitting triple star model of KIC 2856960 with the system parameters constrained to obey Kepler's Laws and to match the binary eclipse width. *Right-panel:* The same data and model, but with the Keplerian constraint removed. The letters label features in the light curve for ease of description in the text.

of Fig. 8. While physically impossible, it is useful to understand how this model manages to match the dips as well as it does. To facilitate our discussion of this we label specific features of the lightcurve using the letters A to F as shown in the right-hand panel of Fig. 8. Further we concentrate upon how the largest star of the binary (star 1) transits star 3 because star 2 in this model plays almost no part in the dips. This is forced by the peculiar absence of any obscuration between minima A and B that we noted in section 3.3.1.

With this simplification, the geometry equivalent to the model of the right-hand panel of Fig. 8 is shown schematically in Fig. 9. As time progresses, the centre of mass of the binary moves from left to right in this figure. Minima in the light curve occur at the points of closest approach (minimum impact parameter) between the centres of stars 1 and 3. The first of these (with significant obscuration) occurs at time A. Remembering that the binary executes its orbit rapidly compared to the advance of the outer orbit, one can see that

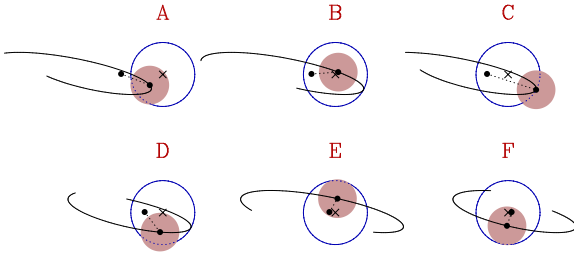


Figure 9. The geometry of stars 1 (small and shaded) and 3 (large and outlined) at the times labelled in Fig. 8, according to the model shown in the right-hand panel of that figure. Star 1 is closer to the observer than star 3 at all times, and is blocking flux from it. The circular dots connected by dotted lines show the centres of mass of star 1 and the binary at the time in question; the cross marks the centre of mass of star 3. The solid curves indicate the path of the centre of mass of star 1 over the range -0.1 to $+0.1$ d relative to the particular time in question. They can be thought of as small sections of the projection of a squashed helix. The orbital inclination of the binary in this model $i_b > 90^\circ$ so that the paths are travelled in a clockwise manner. For clarity we have shrunk the radius of star 1 (solid) by a factor of 2; this does not affect the times of minima / maxima which depend upon the impact parameter only. The precise radius ratio, which controls the depth of the dips, depends also upon the amount of “third light” and is therefore not well defined.

even if one altered the triple phase so that the centre of mass was in a slightly different part of its path, the minimum flux would always be located close to the binary quadrature phase, with the main change being in the amount of overlap of the two stars at the time of minimum. This explains the phenomenology we described when discussing Fig. 6. For instance this is why the dips appear to be locked to the binary rather than the triple phase, and why the first dip is always seen near quadrature.

Times B, C and D span the first of the two double dips, with B and D marking minima and C the intermediate maximum. These three times occur within the same half orbit around quadrature. The single minimum of an A-like event is split into two because while the centre of mass is on the left-hand side of star 3, star 1 moves from the left-hand side to the right-hand side and then back again, leading to two times of minimum impact parameter, with a point close to quadrature where there is a local maximum in the impact parameter, giving a maximum in the flux. Finally, when we have reached the central dips at E and F, the centre of mass of the binary is close to half-way across star 3, meaning that the points of minimum impact parameter are close to the times of binary eclipse.

The explanation of the double dip is important for the discussion of the next section, so in Fig. 10 we show the essential feature of the geometry that leads to double dips in our model. The key point is that the centre of star 1 must cross and re-cross the diameter of star 3 that is approximately perpendicular to the binary star’s line of nodes. This line is vertical in Fig. 10 since we have set $\Omega_b = 270^\circ$ to keep the figure as simple as possible. (Both Figs 9 and 10 are constructed relative to star 3.) On egress from the dips, the same happens in reverse, i.e. the centre of mass of the binary moves to the right of the vertical line in Fig. 10, while star 1 moves from right to left, crossing the vertical dashed line, and then right once more, re-crossing the vertical line for the last time.

Before we leave this section, it is worth noting that we searched hard for hidden parts of parameter space that might resolve the poor fit shown in the left of Fig. 8, but to no avail. The fitting process was well-behaved in that very different starting models would eventually reach the same fit with the same parameters. Thus we are convinced that the left panel of Fig. 8 is the best that a

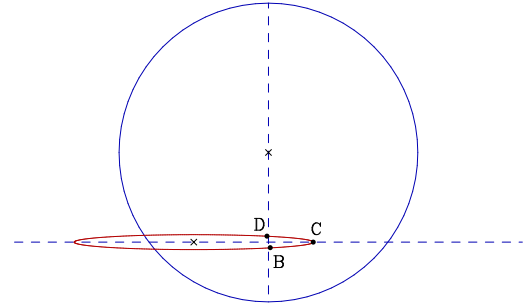


Figure 10. The geometry that leads to the double dips. The ellipse shows the projected motion of the centre of star 1 around the binary’s centre of mass (lower-left cross) which for simplicity we have assumed to be stationary. The circle shows the outline of star 3, and the upper cross its centre. A double dip in the light curve occurs if star 1 crosses the diameter of star 3 marked with the vertical dashed line from left to right and then back again. B and D mark times of minimum flux while C marks a maximum. The binary inclination used here is $i_b = 87^\circ$, and we have aligned the ascending nodes of the binary and triple orbits. The horizontal dashed line indicates the path of the binary’s centre of mass.

physically consistent triple star model can do. For this reason we do not think that KIC 2856960 can be as simple as a triple. In the next section we back up this conclusion with a more analytical treatment of the problem.

3.4 The Dynamical–Geometrical Paradox

Why does the triple model do such a poor job of explaining the dips? In the previous section we found that we could only get somewhere near the data by “relaxing” Kepler’s law, so that the binary separation could become larger (than physically allowable). Obviously this is not acceptable, but the reason for the problem perhaps contains pointers to solving it, and so it is of interest to come to an analytical understanding of it. This also serves as a reassurance that the problems of the previous section are real, and not simply coding errors.

To begin, consider the geometry of Fig. 10. Since the centre of mass of the binary is slowly moving from left to right in this diagram, it is almost inevitable that the circumstance shown will occur at some point during a set of dips. The hard part is to ensure that there are *two* sets of double dips, as widely spaced in time as observed, with the second set mirroring the first during the egress phase of the dips. From Fig. 10, ignoring possible tilts of the orbit relative to the horizontal, this can only happen if the semi-major axis of star 1, a_1 , exceeds half the distance traversed by the centre of mass of the binary between the occurrence of the double dips, which we define to take time Δt . Quantitatively we find that we require

$$\frac{a_1}{a_3 + a_b} > \frac{1 + e_t \cos \nu_t}{\sqrt{1 - e_t^2}} \frac{n_t \Delta t}{2}, \quad (5)$$

where ν_t is the true anomaly of the triple orbit at the time of the dips, which is related to the periastron angle via $\nu_t = 3\pi/2 - \omega_t$. From our fits to the triple’s orbit (section 3.2) we calculate the first term on the right-hand side to be $= 1.449 \pm 0.018$. Using the 4σ lower bound on this factor and setting $\Delta t = 0.7$ d, as measured from the outermost minima of the double dips, one then finds that

$$\frac{a_1}{a_3 + a_b} > 0.0148. \quad (6)$$

Projection factors that arise if the binary’s orbit is tilted with respect

to the triple or problems of exact timing only serve to increase this lower limit.

An alternative limit upon the same quantity is derivable from Kepler’s third law. Eliminating the masses from Eqs 2, 3 and 4 gives

$$\frac{(a_1 + a_2)^3}{P_b^2} = \frac{(a_3 + a_b)^2 a_3}{P_t^2}, \quad (7)$$

which can also be written as

$$\frac{a_1 + a_2}{a_3 + a_b} = \left(\frac{P_b}{P_t}\right)^{2/3} \left(\frac{a_3}{a_3 + a_b}\right)^{1/3}. \quad (8)$$

The final term on the right-hand side is ≤ 1 , while $a_2 \geq 0$, so we deduce that

$$\frac{a_1}{a_3 + a_b} \leq \frac{a_1 + a_2}{a_3 + a_b} \leq \left(\frac{P_b}{P_t}\right)^{2/3} = 0.0117. \quad (9)$$

The upper limit from Eq. 9 (dynamics) is lower than the lower limit from Eq. 6 (geometry). This is the “paradox” of the triple star model of KIC 2856960. There is no room to escape this conflict. Indeed, the equalities in Eq. 9 can only be met if $a_2 \ll a_1$ and $a_b \ll a_3$. We don’t expect either of these to hold true, so even the 0.0117 is likely to be a significant over-estimate. Thus, just as we found with the numerical models, in triple star models one can fit the data (roughly) or Kepler’s laws, but not both with the same model.

A less rigorous constraint, that points in the same direction, but does not rely on our interpretation of the double-dips, can be deduced from the total width of the events which was noted in section 3.3.1 to be $\Delta w \approx 1.4$ d. The maximum width is obtained when all orbits are aligned and star 1 is exactly at quadrature when it first contacts star 3. In that case a similar argument to the constraint that led to Eq. 6 implies that

$$\frac{a_1 + R_1 + R_3}{a_3 + a_b} \geq 0.0296. \quad (10)$$

It becomes difficult to satisfy this and Kepler’s laws without making the ratio of R_1/R_3 so small that one cannot match the dips. For example, if we assume the two stars in the binary are M dwarfs following the typical mass–radius relation of M stars, then a_1 , R_1 and a_3 are determined, and we find that the maximum depth of dips should be $\approx 1\%$ compared to the 8% observed. This is easier to escape than the problem with Kepler’s laws, since an increase in R_1 implies a decrease in R_3 and thus a significant increase in the maximum dip depth, $(R_1/R_3)^2$, but it is suggestive of a similar problem, i.e. that the dips last too long for the triple model to accommodate.

3.5 Quadruple models

Both the problems described in the previous section can be ascribed to a high relative transverse speed between the centre of mass of the binary and star 3. In a triple system this is a simple function of the orbital parameters and, given the light travel time constraints, we have no freedom to alter it. The only plausible way we have thought of to change the transverse speed significantly is by adding a fourth star. If such a star is coupled either to star 3 to form a pair of binaries (which we label “mode 1”, see Fig. 7) or to the close binary to form a hierarchical quadruple (mode 2, Fig. 7), the resultant orbital motion may slow the relative speed between the centre of mass of the close binary and star 3, thereby alleviating the problems of the previous section.

We implemented quadruple models along the lines of the triple star model, and for the first time were able to find solutions that

	M_1	R_1	M_2	R_2	M_3	R_3	M_4
Triple	0.00	1.29	1.28	0.16	1.27	3.89	—
Quad, mode 1	0.50	0.60	0.78	0.16	0.36	0.51	0.91
Quad, mode 2	0.23	0.53	0.42	0.13	1.27	0.40	0.63

Table 3. Masses and radii in solar units of the three types of models for $a_3 = 100 R_\odot$ (the values are taken from the best-fit models for each case). The radius of star 4 is not listed as it is not constrained by any of the models.

qualitatively agree with the data while obeying Kepler’s laws. The fits that result are visually indistinguishable from the right-hand panel of Fig. 8 so we do not show them. The quadruple model is no panacea, but it is the closest we have come to explaining KIC 2856960. The new orbit comes at the cost of a fine-tuning problem since we require its period to be close to an integer divisor of the 204 d period (within ~ 0.001 of an exact integer ratio). This is needed to ensure that the binary occults star 3 at the same part of the new orbit at each set of dips so that the relative speed is always slowed down. If this ratio is not perfect, then at some point in the future one can anticipate considerable changes in the dips, which could change duration or disappear altogether.

In addition to the fine tuning, which is at least not an impossibility, some astrophysical problems remain. Table 3 lists the masses and radii of the three types of models we have considered. The triple model listed is the one forced to obey Kepler’s laws, so that we can define masses consistently, which means that it corresponds to the poor fit of the left-hand panel of Fig. 8. When viewing this table, the unknown value of a_3 which enters into the length that defines the scale, $a_b + a_3$, should be recalled (section 3.3.2), so that all radii are subject to an unknown scale factor s relative to the values listed, and all masses to its cube, s^3 . Since $a_3 > 0$ and we used $a_b = 99.4 R_\odot$ and $a_3 = 100 R_\odot$ in the table, then we can assert that $s > 0.5$, with $s = 1$ for the values listed in the table. Of the three models, the triple model can be ruled out astrophysically as well as from its poor fit to the data, as we noted earlier, since it implies almost zero mass for star 1 ($10^{-5} M_\odot$ to be exact). This comes about from a vain effort to make a_1 as large as possible, at the expense of a_2 to match Kepler’s laws. The small size of star 2 is probably the thorniest issue for the quadruple models. For the mode 1 model, the large mass of star 4 is also a potential problem, since it might end up dominating the light from the system, even though it does not participate in creating the variations seen. However, both quadratic models appear to need significant ($\sim 70\%$) “third light” contributions in addition to the light contributed by stars 1, 2 and 3, so this may not be an impossibility. Otherwise, apart from star 2, the mode 1 mass–radius values look slightly preferable to those of mode 2, although there is not a great deal to choose between them. A final point against mode 2 is that we expect an ≈ 20 second semi-amplitude variations in the light-travel times on the intermediate period (which in our fits lies in the range 5 to 20 d). We searched for such a signal in the light travel times of Fig. 4 and were sensitive to semi-amplitudes of 10 s or more, but did not find anything.

In summary, the quadruple model is shaky, but it does at least not violate basic physics in the same fashion as the triple model when getting close to the data. In implementing the quadruple model, we continued to use hierarchical Keplerian two-body orbits, but it is now much less clear that Newtonian effects can be still neglected. Indeed if the quadruple model is correct, Newtonian perturbations will need consideration to establish the dynamical stability of the system. However, we did not try to add them

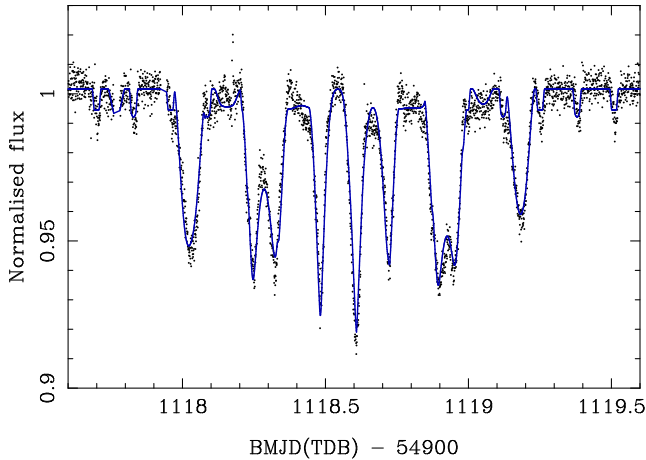


Figure 11. The best mode 1 quadruple model fit to the short cadence dips when the binary epoch T_b is allowed to vary. The χ^2 drops from 13600 to ≈ 9000 , but the model binary eclipses arrive too early compared to the observed ones by ≈ 455 s, a highly significant shift.

because the number of parameters of the quadruple model outstrips our ability to constrain them, and because the poor fit to just the short cadence set of dips alone (during which there would be no significant dynamical evolution) suggests that our model is currently lacking important ingredients beyond N -body perturbations.

3.6 Nagging problems

During our attempts to fit KIC 2856960 two other peculiar problems surfaced that we never resolved. The elusive second component of the binary is one of these. In all the models that provide a reasonable fit to the dips, star 2 is 2.5 to 4 times smaller than star 1. We mentioned this as the chief drawback of the quadruple models in the previous section, because there star 2's small radius is out of kilter with its mass. Such unequal ratios are also not favoured by the binary light curve, although in section 3.2 we argued that star spots made the true ratio uncertain. However, there can be no doubt that the two eclipses in the binary light curve have a similar depth, implying a similar surface brightness for each component of the binary. It is then very hard to understand how these two stars, which are most likely unevolved, low mass main-sequence stars, can differ so much in radius.

Another very puzzling problem concerns the binary ephemeris. None of the models described so far provide a particularly good fit to the data, with, at best, χ^2 values around 13600 for the 4589 points covering the short cadence dips. A very odd feature is that this can be greatly improved, with χ^2 decreasing to ≈ 9000 , simply by letting the close binary epoch T_b vary (Fig. 11). This comes at the significant cost of a mis-alignment between the observed and model binary eclipses. We examined this further by freeing up both T_b and P_b to fit all seven sets of dips simultaneously. Fig. 12 shows the result. This fit returns a significantly longer binary period P_b than obtained from fitting the binary only data (Table 2), with $\Delta P = (3.05 \pm 0.03) \times 10^{-6}$ d, corresponding to 1250 s difference over the time between the first and last dips. This suggests that the offset to the binary ephemeris that best fits the dips changes with time. We have no solution to this curious problem which is perhaps another clue to finding an improved model for KIC 2856960.

We used the triple model without Keplerian constraint to fit all

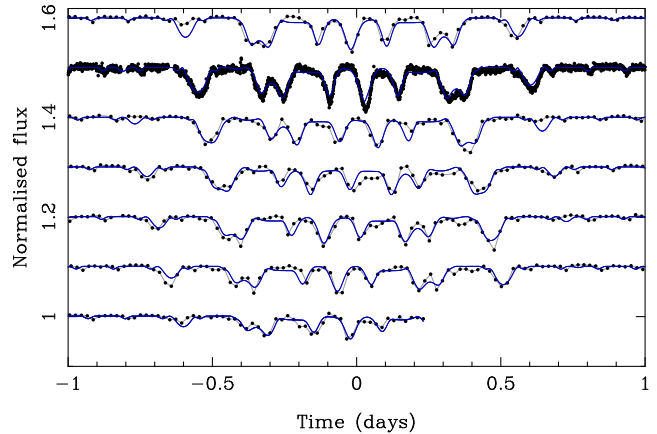


Figure 12. All seven sets of dips together with a mode 1 quadruple model, accounting for finite exposure smearing for the long-cadence data. The binary ephemeris was allowed to vary causing significant mismatches between the model and observed eclipses away from the dips which seem worst for the first set of dips. There is a qualitative match to the seven sets of dips, but also many significant discrepancies.

seven sets of dips in order to establish the ephemeris for the outer orbit which we used when fitting the binary-only data in section 3.2. We found

$$\text{BMJD} = 56018.5661(18) + 204.2723(9)E, \quad (11)$$

where E is an integer, giving the mid-point of the dips, with $E = 0$ coinciding with the set of dips observed in short cadence. We used the triple model because the quadruple model introduces an extra degree of freedom which renders these values much more uncertain, but the possibility of such uncertainty should be borne in mind. Testing for this is a strong reason to attempt ground-based observations of the dips. In using this ephemeris to predict future occurrences of dips, note the use of modified Julian days ($\text{MJD} = \text{JD} - 2400000.5$).

3.7 A spectral type for KIC 2856960

We obtained spectra of KIC 2856960 on the night of May 21, 2012. The spectra were taken during service time, in two sets, three hours apart. The spectrum did not change significantly in this time, and so in Fig. 13 we present the normalised average of the two spectra. We compare these to stars of known spectral type taken from the ELODIE.3.1 library of stellar spectra which contains 1962 spectra of 1388 stars taken with the ELODIE spectrograph at the Observatoire de Haute-Provence 193cm telescope in the wavelength range 390 to 680 nm Prugniel & Soubiran (2001). We used the $R = 42000$ spectra from this library, which we blurred and rebinned to match our data. Fig. 13 shows that KIC 2856960 is dominated by light from a K3 or K4 star. In comparing this with the masses listed in Table 3, the unknown scale factor should be recalled.

4 DISCUSSION

What at first appears to be a fortuitously aligned, but essentially straightforward, triple system, raises a host of problems when one tries to fit the dips that occur when the binary transits its tertiary companion. In some despair, we turned to quadruple star models for the system, although our faith in them is limited as they feel

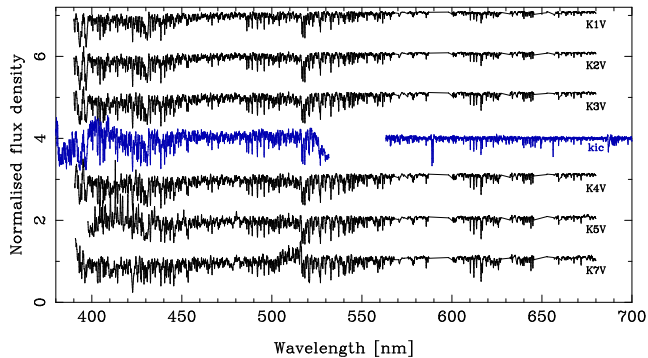


Figure 13. The spectrum of KIC 2856960 (centre) observed with the ISIS spectrograph on the William Herschel Telescope on May 21, 2012, compared to the spectra of main-sequence K stars Prugniel & Soubiran (2001). Some mis-matches are caused by missing data in the templates (at $H\alpha$ and NaI D), and by the dichroic cut between the blue and red arms of ISIS, but otherwise inspection of temperature-sensitive features suggests either a K3 or K4 type for KIC 2856960. We normalised the spectra by spline division and blurred and rebinned the template spectra to match the resolution of the ISIS data.

contrived – epicycles spring to mind. Quadruple models have their own set of problems, although they are less show-stopping than those which afflict the triple model.

Further observations are essential to guide future modelling of KIC 2856960. Spectroscopy over several days could test the binary nature of star 3. Spectroscopy over the 204 d cycle can provide a measurement of a_3 and thus the total system mass. We expect radial velocity variations of several tens of kilometres per second, and the spectrum (Fig. 13) has plenty of sharp line features which should allow precise radial velocities. Spectroscopy at long wavelengths might reveal the close binary. The latter contributes a minimum of $\sim 3\%$ of the light in the *Kepler* bandpass, but this is poorly constrained and could be larger. Even at the minimum contribution, if the stars in the binary are M stars, then given the mid-K star of Fig. 13, we can expect a significantly higher contribution from the binary in the *I*- and *J*-bands. Further monitoring of the dips, possible from the ground given the 8% maximum depth, will also be of value to see whether they evolve significantly with time. If the system is truly a quadruple star, then the simultaneous short, long and intermediate orbital periods, together with the binary eclipses and dips and highly eccentric outer orbit, suggest that it may be of interest for dynamical studies, and significant evolution of the dips can be expected.

5 CONCLUSIONS

KIC 2856960 is an apparent triple star containing a close binary in orbit with another object. Its orientation is such that the close binary passes in front of its companion causing the appearance of a series of dips in the light curve that last for a little over one day and recur on a period of 204 d. The light curve of the binary is consistent with a pair of fairly well detached and similar low-mass M dwarfs. While we expected the system to be straightforward to understand, we were entirely unable to model it as a triple star. Under triple models, the dips can only be modelled with separations of the binary which violate Kepler’s laws. Quadruple star models, involving either two binaries in orbit around each other, or a binary orbited by another star with another star orbiting the three of them, can match the data without straining Kepler’s laws, but require a very near

integral ratio between the 204 d period that the dips recur on and the period of the additional orbit. There are moreover significant remaining mismatches between the model and data even with the extra freedom provided by quadruple systems, and the derived stellar parameters do not seem astrophysically plausible. KIC 2856960 thus defies easy explanation. We urge further observations to uncover the true nature of this remarkable object.

ACKNOWLEDGMENTS

TRM was supported under a grant from the UK’s Science and Technology Facilities Council (STFC), ST/L000733/1. PJC acknowledges support provided by an Early Career Fellowship from the Institute of Advanced Study, University of Warwick. *Kepler* is NASA’s tenth Discovery mission with funding provided by NASA’s Science Mission Directorate. The WHT is operated on the island of La Palma by the Isaac Newton Group in the Spanish Observatorio del Roque de los Muchachos of the Instituto de Astrofísica de Canarias.

REFERENCES

- Armstrong, D., et al., 2012, *A&A*, 545, L4
- Batalha, N. M., et al., 2010, *ApJLett.*, 713, L109
- Carter, J. A., et al., 2011, *Science*, 331, 562
- Conroy, K. E., Prša, A., Stassun, K. G., Orosz, J. A., Fabrycky, D. C., Welsh, W. F., 2014, *AJ*, 147, 45
- Derekas, A., et al., 2011, *Science*, 332, 216
- Eggleton, P. P., Kiseleva-Eggleton, L., 2001, *ApJ*, 562, 1012
- Foreman-Mackey, D., Hogg, D. W., Lang, D., Goodman, J., 2013, *PASP*, 125, 306
- Gies, D. R., Williams, S. J., Matson, R. A., Guo, Z., Thomas, S. M., Orosz, J. A., Peters, G. J., 2012, *AJ*, 143, 137
- Koch, D. G., et al., 2010, *ApJLett.*, 713, L79
- Lee, J. W., Kim, S.-L., Lee, C.-U., Lee, B.-C., Park, B.-G., Hinse, T. C., 2013, *ApJ*, 763, 74
- Naoz, S., Farr, W. M., Lithwick, Y., Rasio, F. A., Teysandier, J., 2013, *MNRAS*, 431, 2155
- Nelder, J. A., Mead, R., 1965, *Computer Journal*, 7, 308
- O’Brien, M. S., Bond, H. E., Sion, E. M., 2001, *ApJ*, 563, 971
- Powell, M. J. D., 1964, *Computer Journal*, 7, 155
- Prugniel, P., Soubiran, C., 2001, *A&A*, 369, 1048
- Prša, A., et al., 2011, *AJ*, 141, 83
- Rappaport, S., Deck, K., Levine, A., Borkovits, T., Carter, J., El Mellah, I., Sanchis-Ojeda, R., Kalomeni, B., 2013, *ApJ*, 768, 33
- Smith, J. C., et al., 2012, *PASP*, 124, 1000
- Stumpe, M. C., et al., 2012, *PASP*, 124, 985
- Thompson, T. A., 2011, *ApJ*, 741, 82
- Torres, G., 2013, *Astronomische Nachrichten*, 334, 4